Transactions of the Materials Research Society of Japan 29 [3] 815-818 (2004)

Electro-Rheological Behavior of Hydrogen-Bonded Liquid Crystalline 4'-*n*-Docosyloxy-3'-nitrobiphenyl-4-carboxylic Acid (ANBC-22) under Sinusoidal Electric Field

Katsufumi Tanaka, Ryuichi Akiyama, Masayuki Takano,
Shoichi Kutsumizu*, and Takanari Yamaguchi**
Department of Polymer Science and Engineering, Kyoto Institute of Technology,
Matsugasaki, Kyoto 606-8585, Japan
Fax: 81-(0)75-724-7800, e-mail: ktanaka@ipc.kit.ac.jp
*Department of Chemistry, Faculty of Engineering, Gifu University, 1-1 Yanagido, Gifu 501-1193, Japan
Fax: 81-(0)58-293-2573, e-mail: kutsu@cc.gifu-u.ac.jp
**Tsukuba Research Laboratory, Sumitomo Chemical Co., Ltd., 6 Kitahara, Tsukuba,
Ibaraki 300-3266, Japan
Fax: 81-(0)29-864-4747, e-mail: yamaguchit9@sc.sumitomo-chem.co.jp

The electro-rheological behavior was studied for 4'-*n*-docosyloxy-3'-nitrobiphenyl-4-carboxylic acid, which is a hydrogen-bonded liquid crystalline material and undergoes a Smectic C (SmC) to Cubic (Cub) phase transition. The electro-rheological behavior was monitored by the dynamic moduli (of the fundamental component when any non-linearity was found) at 404 K, just below the SmC-Cub phase transition temperature under no shear and no electric fields. The storage modulus increased gradually and recovered in response to the application and removal of the sinusoidal electric field, respectively. The loss modulus decreased and recovered. The waveform of the stress response was changed at the same time.
Key words: Electro-Rheology, Liquid Crystals, Hydrogen bond, Smectic Phase, Cubic Phase

1. INTRODUCTION

4'-*n*-Alkoxy- 3'-nitrobiphenyl- 4-carboxylic acids, abbreviated as ANBC-*n* (*n* is the number of carbon atoms in the alkoxy group), are known to exhibit several kinds of aggregation structures such as the smectic phases depending on the alkoxy chain length *n* and temperature, and most notably, three dimensionally ordered cubic (Cub) structures, or (Smectic) D phase, when $n \geq 15$ [1-4]. Recently, the existence of the Cub phase was found in all the higher ANBC homologues from $n = 15$ to $n = 22$ [4] and $n = 26$ [5]. The lowering of the SmC-Cub phase transition temperature and the widening of the temperature range of the Cub phase were also reported with increasing *n*, which make chemical physics studies for the Cub phase much easier [4].

The viscoelastic properties of ANBC-*n* are of great interest, and the storage modulus (*G'*) and loss modulus (*G''*) jump by three orders of magnitude around the transition temperature from the SmC phase to the Cub phase [6,7]. Furthermore, a new application to the stress-transferring device would be open when the transition can be controlled by the external stimuli such as the electric field or the magnetic field as well as the mechanical field. Rheological responses to the external electric field, the ER effect [8-11], have been reported for smectic liquid crystals [9-11]. These results are closely related to the orientation of layered structures with respect to the flow direction, packing of molecular axes with polar groups in the layer, and macroscopic anisotropic textures developed in the smectic phases. Especially, the dielectric anisotropy, $\Delta\varepsilon$ ($= \varepsilon_{//} - \varepsilon_{\perp}$, where $\varepsilon_{//}$ and $\varepsilon_{\perp}$ are, respectively, the dielectric constants measured parallel and perpendicular to the long axis of the molecule), is an important factor for the ER effect.

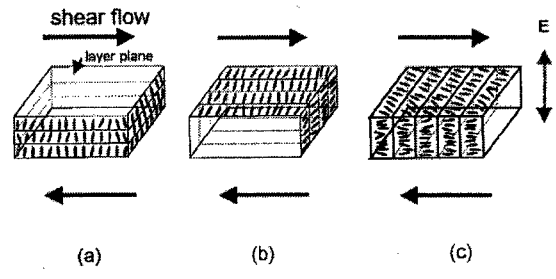

Fig.1 Characteristic geometries for a sheared smectic liquid crystal with a negative dielectric anisotropy; (a) velocity parallel and gradient perpendicular to the layers, (b) velocity parallel and gradient parallel to the layers, and (c) velocity perpendicular and gradient parallel to the layers. Sinusoidal external electric field is applied as shown by the arrow.

Fig.1 shows characteristic geometries for a sheared (monodomain) smectic liquid crystal [12] with $\Delta\varepsilon < 0$. When the liquid crystal with orientation (a) (or (b)) is sheared under no electric field, the flow will be easily induced because of the slippage at the interlayer of the layered structure. On the other hand, the flow resistance, or the (apparent) viscosity, would be larger when the liquid crystal with orientation (c) is sheared. The positive ER effect, which is an increase in the apparent viscosity induced by the electric field, for Smectics with $\Delta\varepsilon < 0$ can possibly be explained by the switching by the electric field from orientation (a) (or (b)) to orientation (c). In a polydomain texture [9] of Smectics, inter-domain interactions would be also an important factor. However, the electro-hydrodynamic instability [8], which sometimes affects the ER effect for much lower order liquid crystals such as Nematics or Cholesterics induced by the DC electric field or the sinusoidal electric field with sufficiently low frequencies, is mostly negligible because the viscosity of Smectics is much larger than that of Nematics or Cholesterics.

For ANBC-22 having Cub phases that are much more highly ordered but energetically close to the low-temperature SmC phase, a new feature of the ER effect induced by the phase transition is expected. In the present paper, the ER effect of ANBC-22 just below the SmC-Cub phase transition temperature under no shear and no electric fields was investigated preliminarily.

2. EXPERIMENTAL

ANBC-22 studied here was prepared at Gifu University by essentially the same method as that of Gray et al. [1] and the previous report [6]. The differential scanning calorimetry (DSC) trace shows the following phase sequence on the first heating at 5 K min^{-1}, where the onset temperatures are shown instead of peak temperatures: Crystal 373 K SmC 410 K *Im3m*-type Cub {ca. 453 K} *Ia3d*-type Cub 468 K Isotropic Liquid I (I_1) (476 K) Isotropic Liquid II (I_2). The peak temperature for the I_1 to I_2 transition is shown in parentheses because of the overlap with the preceding transition. The *Im3m*-type Cub to *Ia3d*-type Cub phase transition, the temperature of which is shown in braces, was detected by small-angle X-ray scattering (SAXS) [5], viscoelastic [6] and adiabatic calorimetric [13] measurements but not by DSC. Identification of the phase type shown here was also performed by texture observation using a polarized optical microscope (POM).

Here, it should be noted that the SmC and Cub phases as well as the two Cub phases are energetically close to each other [13]. In the present study, we focus our attention on the SmC phase just below the phase transition temperature to *Im3m*-type Cub phase on heating. The onset temperature of the SmC to *Im3m*-type Cub transition determined by POM was 406 K on the first heating.

Dielectric relaxation measurements were also performed at Gifu University with an LCR meter (HP-4274A). The frequency range was between 100 Hz and 100 kHz and the temperature was 396 K, at which ANBC-22 shows the SmC phase. The cell gap was 100 μm.

The viscoelastic measurements with small oscillatory shear strain were performed with a rotational rheometer (Rheology Co., Ltd., MR-300V2E) with a fixture of parallel plates. The sinusoidal electric field was also applied to the samples sandwiched between the parallel plates (electrode). The details of the electro-rheological measurements were reported elsewhere [8,9]. In the present study, the gap distance between the parallel plates was set to be 200 μm. Sufficient care was taken that the temperature of the parallel plates was kept below 394 K during the sample insertion. After the sample was completely sandwiched, the temperature was raised carefully to 404 K and kept for more than one hour prior to the measurements. The angular frequency of the oscillatory shear strain was fixed to be 9.42 rad s^{-1}, while the smaller amplitude of 0.024 and the larger amplitude of 0.12 of the strain were applied. The sinusoidal electric field with an amplitude of 10 kV mm^{-1} and a frequency of 10 kHz was applied to the sample and then removed during the measurement. The waveforms of the stress and strain were also measured at the same time. In case of the non-linear response, the fundamental component of the torque amplitude was extracted from the distorted torque wave, and the fundamental components of the dynamic moduli G_1' and G_1'' were calculated [14].

3. RESULTS AND DISCUSSION

3.1 POM Observation and Dielectric Relaxation of ANBC-22

Fig. 2 shows POM micrographs of ANBC-22 in the quiescent state, (a), and in the sheared state, (b). ANBC-22 was sandwiched between a slide glass and a cover glass (with no spacer) at 483 K in the isotropic liquid phase and cooled slowly to room temperature. The sandwiched sample was heated again to 403 K and kept at the temperature for about 15 min. As shown in Fig. 2 (a), a fine grain-like anisotropic texture was observed. The sample was slightly sheared manually at the temperature, and then a layered texture was developed remarkably as shown in Fig. 2 (b).

In the dynamic viscoelastic measurements at 404 K described in the next section, similar changes in the anisotropic texture would be induced by the oscillatory shear strains with the larger amplitude of 0.12.

Fig.3 shows the dielectric constant and loss of ANBC-22 in SmC phase plotted against the frequency. In the figure, a dielectric relaxation behavior is found in the frequency range 0.1-1 kHz, but the dielectric loss is almost zero above 10 kHz. Therefore, the electrical heating caused by the conduction current was negligible at frequencies above 10 kHz.

In the present study, the sinusoidal electric

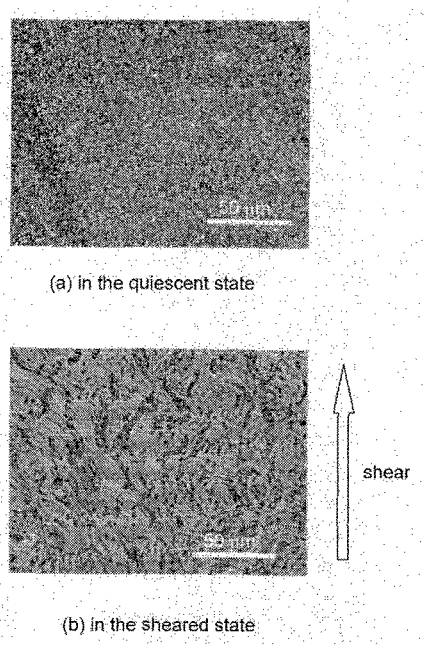

Fig. 2 Polarized optical micrographs of ANBC-22 at 403 K (a) in the quiescent state and (b) in the sheared stated.

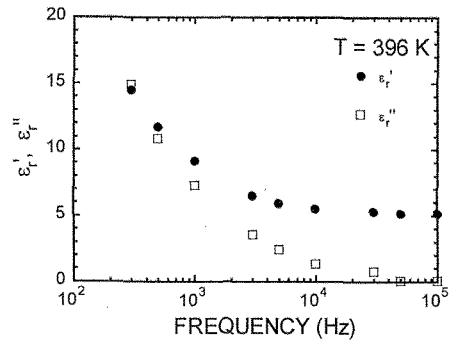

Fig.3 Dielectric constant and loss of ANBC-22 in SmC phase at a temperature of 396 K plotted against the frequency of electric field.

field with the frequency of 10 kHz was applied to ANBC-22 during the dynamic viscoelastic measurement. Furthermore, the POM observation under the sinusoidal electric field showed no convection caused by the electro-hydrodynamic instability at frequencies including 10 kHz [15].

3.2 Responses of Dynamic Viscoelastic Moduli to the Sinusoidal Electric Field

Figs. 4 (a) and (b) show, respectively, plots of the storage and loss moduli against time, which were measured at 404 K with the smaller and the larger amplitudes of strain. The sinusoidal electric field was also applied to the sample in the time interval between 1000 s and 1500 s during the measurements. In Fig. 4 (a), G' measured with $\gamma_0 = 0.024$ is around 980 Pa and it is almost constant before application of the electric field. With the same amplitude, in Fig. 4 (b), a similar tendency is seen for G''.

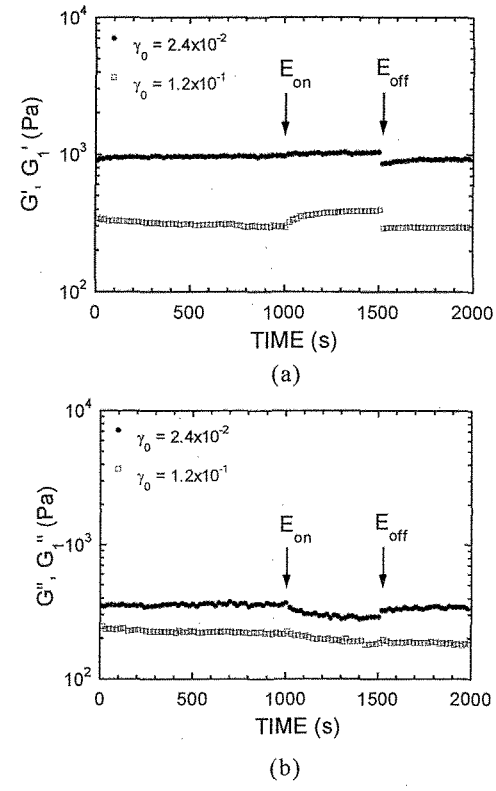

Fig. 4 (a) Storage moduli and (b) loss moduli plotted against time under two strain amplitudes γ_0. The electric field was applied to the sample in the time interval indicated by two arrows.

As discussed later, the stress response to the smaller strain amplitude under no electric field was well assumed to be linear. However, the waveforms of the stress response to the larger strain amplitude and the waveforms under the electric field were distorted, where the obtained parameters are G_1' and G_1'' [14]. When measured with $\gamma_0 = 0.12$, in Fig. 4 (a), G_1' is initially around 350 Pa under no electric field and it gradually decreases to around 300 Pa just before the application of the electric field. A similar drift is also seen for G_1'' in Fig. 4 (b).

After application of the electric field, in Fig. 4 (a), G_1' measured with $\gamma_0 = 0.024$ increases slightly, while G_1'' in Fig. 4 (b) decreases. On the other hand, G_1' measured with $\gamma_0 = 0.12$ increases much more significantly, while G_1'' decreases. Furthermore, sufficiently after removal of the electric field, G' (or G_1') and G'' are well recovered to the values just before application of the electric field. However, G_1'' measured with $\gamma_0 = 0.12$ after removal of the electric field is a little smaller than G_1'' just before application of the electric field.

Fig. 5 shows examples for Lissajous figures of the oscillatory stress and strain (in short, the stress-strain loop) with $\gamma_0 = 0.024$, which were monitored through the measurements. In the figure, the extracted fundamental stress-strain loops are also plotted.

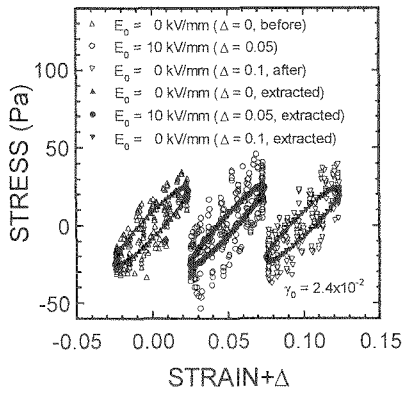

Fig. 5 Lissajous figures of the stress and strain measured with $\gamma_0 = 0.024$. The figures during the application of the electric field (just before the removal) and after the removal are shifted to the larger strains, Δ. The extracted fundamental stresses (solid symbols) are also plotted.

The stress-strain loop under the electric field, which was monitored just before removal of the electric field, is different from the other loops under no electric field. The amplitude of the stress-strain loop under the electric field is larger than the amplitudes under no electric field. Furthermore, the waveform of the stress under the electric field was slightly distorted. No such distortion of the waveforms under the electric field was found for a silicone oil of 50 Pa s, which shows no ER effect. In Fig. 5, changes in the extracted stress-strain loop with the electric field are less pronounced but detected, which corresponds to the slight changes in the dynamic moduli shown in Figs. 4 (a) and (b). Similar tendencies of the stress-strain loops were found with the larger amplitude of the strain. In this case, the waveforms of the stress under no electric field as well as under the electric field were distorted. As reported elsewhere, the electric field induces the formation of a Cub phase just below the transition temperature under no deformation [15]. Therefore, the electric field favors the growth of the Cub phase even in the SmC phase, but the larger strain amplitude stabilizes the SmC layered structure as seen for the sheared sample in Fig. 2 (b), both of which would cause the deformation of the waveforms and also would enhance the change in G_1' with the application and removal of the electric field. With the smaller strain amplitude, on the other hand, the texture of the SmC phase would be almost identical to the texture shown in Fig.2 (a) during the dynamic measurements.

At present, we assume the contribution of $\Delta\varepsilon$ (< 0) to the ER effect as shown in Fig.1 is small, because dimerization of two ANBC-22 molecules with the anti-parallel orientation would reduce the macroscopic polarity, and thus the absolute value of the dielectric anisotropy cannot be large enough to rearrange the anisotropic domains macroscopically. Rather, the main origin of the ER effect would be the electric field-induced SmC-Cub transition. However, the increase in G' (or G_1') induced by the electric field was not so large in the present study as reported at the same transition but under no electric field [6,7]. Under the POM observations using a gap of 4 μm (with no deformation), the completion of the electric field-induced SmC-Cub transition at 400 K required more than 10 min [15]. In the present study, the sinusoidal electric field was almost the same as used in Ref [15], but the gap between the electrodes was as wide as 200 μm. A remarkable increase in the bulk storage modulus is expected only when the Cub phase develops substantially to chain between the electrodes. It is probable that the growth of the Cub phase is confined heterogeneously just adjacent to the electrodes; the time required for the completion of the field-induced transition can be much longer than that required for POM observation.

A combination of applying electric field and shear strain is promising for controlling the SmC-Cub phase transition of ANBC-22, but fine tuning of several factors such as strain amplitude γ_0, the gap, etc. is necessary. Further studies are in progress to overcome these problems.

References

[1] G.W. Gray, B. Jones and B. F. Marson, *J. Chem. Soc.*, 393-401 (1957) .
[2] D. Demus and G. Kunicke, J. Neelsen, H. Sackmann, *Z. Naturforsch., Teil A*, 23, 84-90 (1968).
[3] D. Demus, D. Marzotko, N. K. Sharma and A. Wiegeleben, *Kristall. Technol.*, 15, 331-39 (1980).
[4] S. Kutsumizu, M. Yamada and S. Yano, *Liq. Cryst,*. 16, 1109-13 (1994).
[5] S. Kutsumizu, K. Morita, T. Ichikawa, S. Yano, S. Nojima and T. Yamaguchi, *Liq. Cryst.*, 29, 1447-58 (2002).
[6] T. Yamaguchi, M. Yamada, S. Kutsumizu and S.Yano, *Chem. Phys. Lett.*, 240, 105-08 (1995).
[7] S. Kutsumizu, T. Yamaguchi, R. Kato and S. Yano, *Liq. Cryst.*, 26, 567-73 (1999).
[8] K. Tanaka, A. Takahashi, R. Akiyama and N. Kuramoto, *Phys. Rev. E.*, 59, 5693-96 (1999).
[9] K. Tanaka, Y. Oiwa, R. Akiyama and A. Kubono, *Polym. J.* (Tokyo), 30, 171-76 (1998).
[10] M. Fukumasa, K. Yoshida, S. Ohkubo and A. Yoshizawa, *Ferroelectrics*, 147, 395-09 (1993).
[11] K. Negita, *Int. J. Mod. Phys. B*, 13, 2005-10 (1999).
[12] P. G. de Gennes and J. Prost, "The Physics of Liquid Crystals", 2nd Ed., Oxford (1993) Ch. 8.
[13] K. Saito, T. Shinhara, T. Nakamoto, S. Kutsumizu, S. Yano and M. Sorai, *Phys. Rev. E*, 65, 031719-1-7 (2002).
[14] S. Onogi, T. Masuda and T. Matsumoto, *Trans. Soc. Rheol.*, 14, 275-94 (1970).
[15] S. Kutsumizu, M. Yamada T. Yamaguchi, K. Tanaka and R. Akiyama, *J. Am. Chem. Soc.*, 125, 2858-59 (2003).

(Received October 14, 2003; Accepted March 12, 2004)